Journal of Applied Electrochemistry (2006) 36:1361–1366
DOI 10.1007/s10800-006-9199-7

Investigation of Ti mesh-supported anodes for direct borohydride fuel cells

H. CHENG* and K. SCOTT
School of Chemical Engineering & Advanced Materials, University of Newcastle upon Tyne, NE1 7RU, Newcastle upon Tyne, UK
*(*author for correspondence, fax: + 44-0191-222-5292, e-mail: hua.cheng@ncl.ac.uk)*

Received 27 February 2006; accepted in revised form 22 June 2006

Key words: direct borohydride fuel cell, borohydride oxidation, Ti mesh, anode catalyst

Abstract

The use of titanium mesh-supported gold and silver anodes in direct borohydride fuel cells (DBFCs) is reported. The anodes were prepared by either thermal decomposition or electrochemical deposition and were characterised by scanning electron microscopy and X-ray diffraction analyses. The performance of the mesh electrodes was compared with that for carbon-supported electrodes. The mesh anodes gave current densities, for borohydride oxidation, up to 50% greater and cell power densities up to 20% greater than those obtained with carbon-supported anodes. The effects of catalyst loading and fuel cell operating conditions are also reported. Electrode stability was examined over a prolonged period.

1. Introduction

The direct borohydride fuel cell (DBFC) has attracted growing interest as a potential high power source for a range of transportation and stationary power applications [1–7]. One reason for the interest is its high theoretical open circuit voltage of 1.64 V, which is approximately 0.43 V higher than that of the direct methanol fuel cell (DMFC). The electrode and cell reactions with the associated standard potentials (vs. SHE) are:

Anode:

$$BH_4^- + 8OH^- = BO_2^- + 6H_2O + 8e^- \quad E^0 = -1.24\,V \tag{1}$$

Cathode:

$$2O_2 + 4H_2O + 8e^- = 8OH^- \quad E^0 = 0.40\,V \tag{2}$$

Overall:

$$BH_4^- + 2O_2 = BO_2^- + 2H_2O \quad E^0 = 1.64\,V \tag{3}$$

Since an inorganic fuel is used, the DBFC benefits from the absence of the CO-poisoning of the anode catalysts, associated with the use of hydrogen reformate fuels or organic based fuels. In addition, borohydride and its oxidation products are less toxic in contrast to alternative inorganic fuels such as hydrazine.

Progress in the development of DBFCs has been reviewed in terms of the importance of operating parameters on cell performance and the advances in technology [1, 2]. The DBFC was compared to the DMFC and the indirect borohydride fuel cell that uses hydrogen generated catalytically via the borohydride hydrolysis reaction [1, 2]. The requirements for synthesising new electrocatalysts for borohydride oxidation are also highlighted [1]. A possible limitation for the practical application of the DBFC, i.e., a strongly alkaline supporting electrolyte is required to prevent the hydrolysis of borohydride, has been mentioned [1].

The mechanism and kinetics of borohydride oxidation have been investigated using fundamental electrochemical techniques such as cyclic voltammetry and rotating disk electrode [8–12]. Gold and gold alloys, e.g. carbon-supported Au and Au (97 wt%)/Pt (3 wt%) alloy, have been identified as effective catalysts for borohydride oxidation [13]. Incomplete oxidation of borohydride has been reported [5, 6]. The measured numbers of electrons involved in the oxidation are values between 2 and 6 for Pt [5, 14], Ni [5, 15], Pd [5] and hydrogen storage alloys such as $Zr_{0.9}Ti_{0.1}Mn_{0.6}V_{0.2}Co_{0.1}Ni_{1.1}$ [6].

Direct borohydride fuel cells with various geometric configurations have been developed [3–7, 13, 16]. A conventional electrode structure, consisted of successive catalyst layers, a microporous layer and carbon paper, was used in our previous work [7]. Such a structure causes relatively high diffusion resistances for fuel mass transport and for release of gas produced from the side reaction:

$$BH_4^- + 2H_2O = BO_2^- + 4H_2 \tag{4}$$

Carbon powder is also susceptible to gradual electrochemical oxidation at the high potentials which can

occur in the DBFC [17]. In this regard, Ti mesh is a promising alternative catalyst support due to its acceptable electronic conductivity, high chemical and electrochemical stability, open structure and ease of fabrication into electrodes. The aim of this work was, therefore, to examine the feasibility of using Ti mesh-supported anodes in DBFCs. Gold and silver catalysts were chemically or electrochemically deposited on Ti mesh substrates and the effect of the preparation conditions were investigated. The electrochemical behaviour of the mesh anodes was evaluated and compared to carbon-supported anodes. To the authors' knowledge, this is the first investigation of using silver as an anode catalyst and Ti mesh as a catalyst support in the DBFC, although the mesh support has been used in electrochemical reactors [18] and in the direct methanol fuel cells [19, 20].

The study used standard carbon-supported Pt catalysts as cathode materials, which are commonly used by most researchers. However, alternative cathode catalysts such as MnO_2 have been explored [21], although these catalysts are not as active as Pt.

2. Experimental

2.1. *Preparation and characterisation of materials*

Titanium mesh (99.6%, nominal aperture: 0.19 mm, open area 20%, wire diameter 0.23 mm, Goodfellow) supported anodes were prepared, using the reported thermal deposition procedure [22], at deposition temperatures of 400 °C and 600 °C for Au and Ag catalysts, respectively [23]. The catalyst coated mesh was post-treated cathodically by electrolysis at −1.2 V versus Hg/Hg_2SO_4-saturated K_2SO_4 (Russell) in a 0.5 M NaOH (99.99%, Aldrich) aqueous solution for 1 h, which transformed all oxides to metal electrodes. The Au catalysts were also prepared by electrodeposition onto the Ti mesh, at a current density of 1 mA cm^{-2}. In this case, a solution of 0.1 M H_2SO_4 (98%, BDH) and $AuCl_3$ (99%, Aldrich) was used. The typical concentrations of $AuCl_3$ used were 0.1–0.2 M and the amount of $AuCl_3$ was added according to loading requirements. The deposited materials were treated in air at 500 °C for 1 h to decompose oxides completely [23].

Carbon-supported Au, Ag and Pt catalysts were prepared following the impregnation method [24] using $AuCl_3$, $AgNO_3$ (99.9%, Aldrich) and H_2PtCl_6 (99.9%, Janssen) as catalyst precursors. For example, 200 mg of carbon powder (Vulcan XC-72R, Cabot) was dispersed in a mixture of isopropanol and deionised water (volume ratio 1:1, 20 cm^3) at 60 °C under magnetic stirring for 10 min. Then, 185 mg of $AuCl_3$ was added dropwise and stirred for another 1 h. The mixture was filtered and the resultant slurry was washed with water and dried at room temperature before thermal treatment, at 500 °C for 1 h, in air.

Scanning electron microscopy (SEM) was carried out using a JEOL JSM-5300LV scanning electron microscope at an acceleration voltage of 25 kV. X-ray diffraction (XRD) analysis was performed with a Siemens D-5005 X-ray Diffractometer using Cu Kα radiation. The tube current was 100 mA and the tube voltage was 40 kV. The 2θ angular regions between 10° and 120° were explored at a scan rate of 2° min^{-1}. The XRD pattern was compared to the International Centre for Diffraction Data® (ICDD®) [25].

2.2. *Half cell test*

A Sycopel potentiostat system (25 V, 3 A, Sycopel Scientific Limited) and an undivided three-electrode glass cell (Figure 1, 200 cm^3 in volume) were used for polarisation measurements. The circular mesh anode was placed inside a Teflon holder provided with a platinum-ring current collector and a channel for passing nitrogen gas (BOC) through the electrolyte before measurements. The anode (1 cm^2 in geometric area) kept a distance of 0.5 cm to the counter electrode. For comparison, carbon-supported gas diffusion electrodes were prepared by pasting a mixture of the catalyst, Nafion (30 wt% of the catalyst, using a 5 wt% Nafion solution from Aldrich) and isopropanol onto carbon paper (Toray, TGPH120, E-TEK) and then hot-pressing at 100 kg cm^{-2} and 130 °C for 3 min. All working electrodes were pre-treated electrochemically in a 1 M NaOH solution at potentials between −1.5 and 0.6 V versus Hg/Hg_2SO_4-saturated K_2SO_4 at a scan rate of 50 mV s^{-1} for 20 cycles.

2.3. *Fuel cell test*

To fabricate a membrane electrode assembly (MEA), the cathode was first hot-pressed onto one side of the Nafion® 117 membrane (DuPont) at 100 kg cm^{-2} and 130 °C for 3 min. The Au/Ti mesh and the Ni mesh (99.0%, nominal aperture: 0.25 mm, open area 36%, wire diameter 0.17 mm, Advent) were then bound up into one piece using a PTFE tape (2 mm in width) along the mesh edges. The meshes were dipped twice into the 5% Nafion solution before hot-pressing onto the other side of the membrane at 100 kg cm^{-2} and 130 °C for 3 min. The Ni mesh was sandwiched between the membrane and the Au/Ti mesh electrode to ensure greater contact of the electrolyte and the Au catalysts and to facilitate better gas release, if hydrogen was formed by hydrolysis of $NaBH_4$. The MEA was assembled between graphite blocks (Ralph, Coidan) with parallel flow channels (1 mm in width and 1 mm in depth) gave an electrode active area of 4 cm^2. Copper sheets contacted the graphite blocks as current collectors. Electrical heaters were mounted at the rear of the Cu plates to maintain the required cell temperature.

Steady-state polarisation measurements were carried out after a 10 h conditioning, during which the cell was

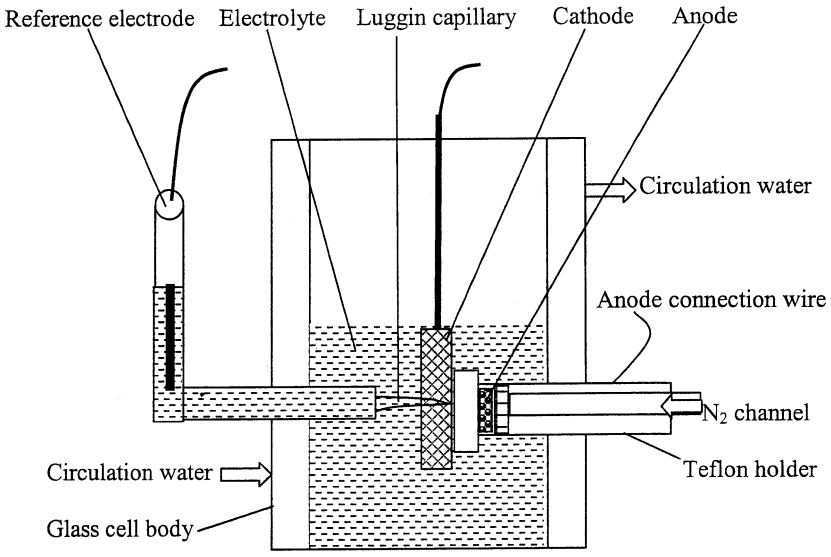

Fig. 1. Schematic diagram of an undivided cell.

held at 60 °C and both flow channels were fed first with deionised water for 5 h and then the anode flow channel was fed with a 1 M NaOH solution for another 5 h. Polarisation curves were recorded in a galvanostatic mode, starting from open circuit point and moving to higher current densities. Other details of the MEA fabrication and the DBFC operation are reported elsewhere [7, 19].

3. Results and discussion

3.1. *Structural characteristics*

Figure 2 shows a typical SEM for the Au/Ti mesh electrode. A well-dispersed deposit of Au particles, with a wide range of particle sizes, can be observed. The XRD image (Figure 3) shows the high degree of crystallinity of the Au particles with a cubic structure. The peak diffraction angles correspond to the Au(111), Au(200), Au(220), Au(311) and Au(222) crystal faces, which match well with the standard Au peaks [25]. Also peaks corresponding to the Ti(101), Ti(102) and Ti(103) crystal faces are observed at diffraction angles of 40.1, 53.1 and 70.7°, respectively.

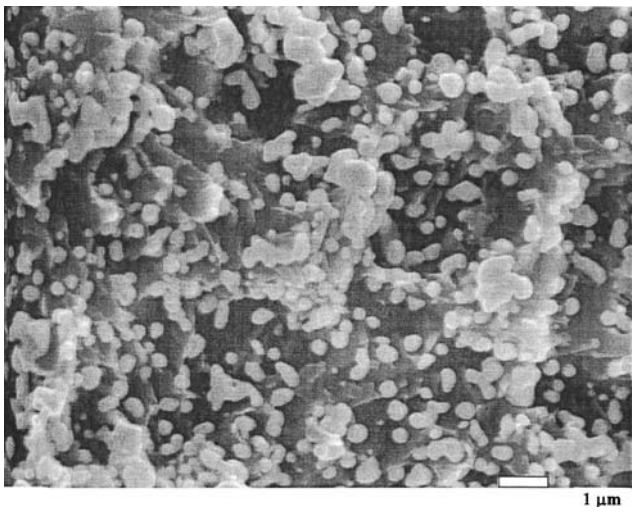

Fig. 2. SEM of the Ti mesh-supported Au material at a magnification of 10,000.

3.2. *Half cell evaluation*

Figure 4 shows linear sweep voltammograms for the Ti mesh-supported Au and Ag anodes (Au/Ti and Ag/Ti), in a solution of 1 M $NaBH_4$ and 1 M NaOH; where the potentials were measured against the Hg/Hg_2SO_4-saturated K_2SO_4 reference electrode. The data obtained on the carbon-supported Au anode (Au/C) are also included for comparison. As can be seen, borohydride oxidation on these anodes starts at a very negative potential (ca. −1.5 V). Oxidation current densities increase rapidly after −0.8 V and the Au electrode is found to be more active than the Ag electrode. The

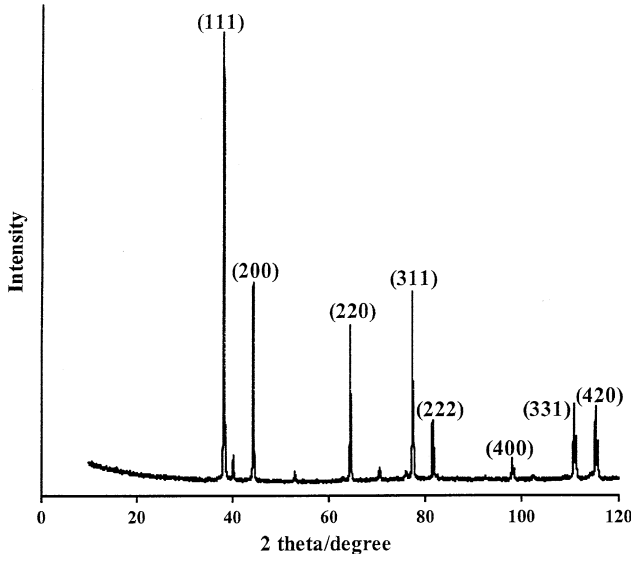

Fig. 3. XRD of the Ti mesh-supported Au material.

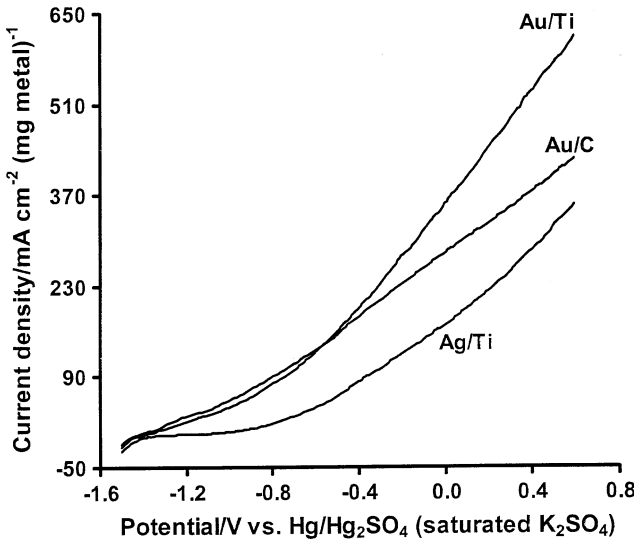

Fig. 4. Linear sweep voltammogram at the Ti mesh- or carbon-supported anodes (1.0 cm^2) in a solution of 1 M $NaBH_4$ and 1 M NaOH. Cell: undivided cell. Catalyst loading: 1 mg metal cm^{-2}. Counter electrode: Pt mesh (20 cm^2). Scan rate: 50 mV s^{-1}. Temperature: 20 ± 0.1 °C.

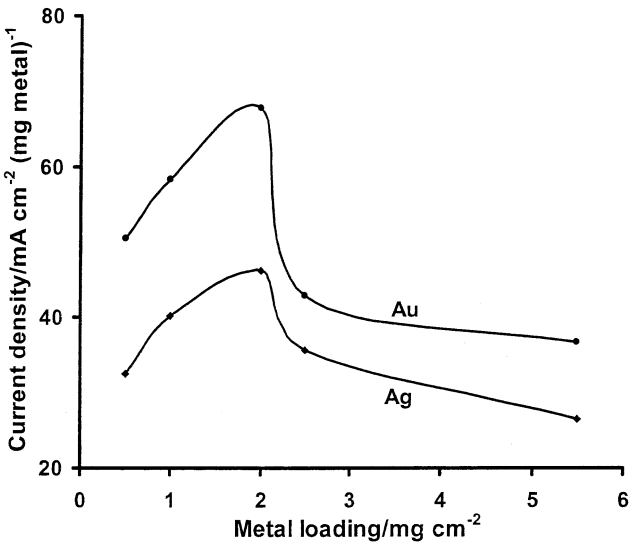

Fig. 5. The effect of catalyst loading on the anode activity for borohydride oxidation. Anode catalyst: Au or Ag cm^{-2}. Controlled potential: −0.8 V versus Hg/Hg_2SO_4-saturated K_2SO_4. Other conditions as in Figure 4.

carbon-supported Au electrode shows better performance than the titanium-supported Au electrode at potentials below −0.6 V. At low potentials, mass transport of borohydride does not limit oxidation on the Au/C; highly dispersed catalysts on the carbon support result in higher catalyst utilisation, leading to better performance, compared to the Au/Ti. At higher potentials, the Au/Ti electrode gave better performance than the Au/C electrode, i.e., greater current densities at fixed potential. This is a result of limitations in borohydride mass transport which are expected to be more severe for the Au/C electrode than the Au/Ti mesh electrode due to latter's more compact structure.

Figure 5 shows the effect of catalyst loading on the borohydride oxidation current densities, at a potential of 0.8 V versus Hg/Hg_2SO_4-saturated K_2SO_4. As can be seen, the current density does not increase with the catalyst loading over the range considered but gives a maximum with a loading of 2 mg metal cm^{-2}. At higher loadings, a thicker electrode can suffer from poorer current distribution which limits the catalyst utilisation. In addition, the catalyst particles may be larger and block adjacent active sites to further lower catalyst utilisation. The Ag catalyst displays similar behaviour but lower activity than the Au catalyst at all loadings.

The two methodologies for mesh anode preparation using electrochemical deposition and thermal decomposition, exhibit similar behaviour, e.g., similar current densities at fixed potential.

3.3. *Fuel cell performance*

3.3.1. *Influence of catalyst and anode support*

Figure 6 shows typical fuel cell voltage and power density versus current density data collected from the DBFCs with the Au/Ti and Ag/Ti anodes. As can be seen, the DBFC with the Au/Ti shows the superior fuel cell performance to that with the Au/C at current densities above 50 mA cm^{-2}. A peak power density of 81.4 mW cm^{-2} is observed for the DBFC with the Au/Ti anode. It is encouraging that the non-precious metal Ag anode delivers power densities of up to 50 mW cm^{-2}.

The influence of anode catalyst loading on the DBFC performance is shown in Figure 7. For the Au anode, the power density increases by over 25% when the Au

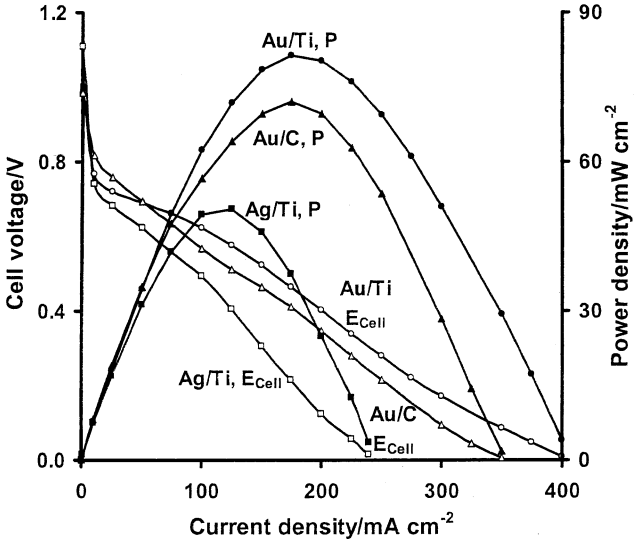

Fig. 6. Steady cell voltage (E_{Cell}) and power density (P)-current density curves collected from the DBFCs with different anodes. Active area: 4 cm^2. Anode loading: 2 mg metal cm^{-2}. Cathode: Pt/C (2 mg Pt cm^{-2}). Membrane: Nafion® 117. Flow field: parallel flow field. Fuel: a solution of 1.32 M $NaBH_4$ and 2.5 M NaOH (flow rate: 10 cm^3 min^{-1}). Oxidant: O_2 (ambient pressure, 200 cm^3 min^{-1}). Temperatures: 85 °C.

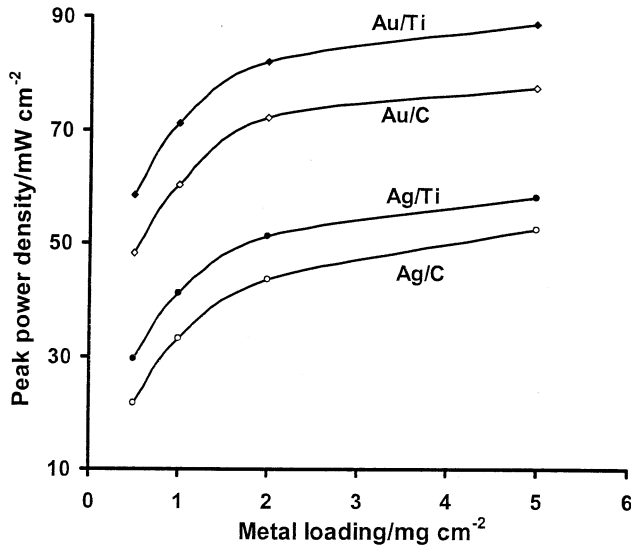

Fig. 7. The effect of catalyst loading on the peak power density. Anode catalyst: Au or Ag cm^{-2}. Other conditions as in Figure 6.

loading increases from 0.5 mg Au cm^{-2} to 2 mg Au cm^{-2}. A further increase in catalyst loading has a relatively small effect on the fuel cell performance. It seems that the anode capability towards borohydride oxidation is low at low metal loadings. The relatively poorer performance at high loadings implies that the thick catalytic layer has an adverse effect on internal resistances, mass transport of borohydride and diffusion of gas products.

The performance of the DBFC with the Ag anode displays a similar behaviour as that obtained with the Au anode. The DBFC with the Ag anode produces a 70% increase in power density, from 30 mW cm^{-2} to 50 mW cm^{-2} for an increase in loading from 0.5 mg cm^{-2} to 2 mg cm^{-2}. Overall, it appears that a loading of 2 mg metal cm^{-2} gives an optimum performance of the DBFC. The data generally confirm the trend observed in the half cell measurements and demonstrate the advantages of using the mesh support over the carbon support in terms of power performance.

Figure 7 also shows that the DBFCs with the Ti mesh-supported anodes are superior to those with the carbon-supported anodes for both Au and Ag catalysts and at all loadings. This is because the very open structure of the mesh allows better borohydride mass transport and faster gas bubble release than the bounded carbon-supported anodes. Overall the Ti mesh appears a promising anode support for the DBFC.

3.3.2. *Influence of fuel conditions*

Table 1 shows the influence of $NaBH_4$ concentration and cell temperature on the performance of the DBFC with the Au/Ti anode. As shown in Table 1, increases in cell temperature and borohydride concentration gives higher power densities and higher sustained current densities, presumably due to the improved mass transfer of the reactants and to the decreased activation and concentration overpotentials. The peak power density

Table 1. Effects of temperature and $NaBH_4$ concentrations on open circuit voltage (OCV), peak power density (P_{Peak}) and sustained maximum current density (j_{Max})[a]

Conditions	1.32 M $NaBH_4$				85 °C		
	25 °C	50 °C	70 °C	85 °C	0.80 M	2.64 M	3.28 M
OCV/V	1.05	1.04	0.99	0.98	0.98	0.95	0.94
P_{Peak}/mW cm^{-2}	26.8	53.0	62.5	81.4	65.3	89.5	92.4
j_{Max}/mA cm^{-2}	120	200	260	400	300	420	435

[a]The Au/Ti anode. Other conditions as in Figure 6.

increases by 25% with increasing borohydride concentration from 0.80 M to 1.32 M, above which the value increases by 10–15%. The increased conductivity of a solution of borohydride and sodium hydroxide with increasing temperature [26] also promotes better performance. The negative effect of increasing temperature and borohydride concentration on the open circuit voltages is also shown in Table 1. This mainly results from the increased borohydride crossover, which has the enhanced detrimental effect on the cathode performance. The best DBFC performance is achieved using a fuel of 1.32 M $NaBH_4$ and 2.5 M NaOH at 85 °C.

3.3.3. *Durability test*

A key to commercial implementation of the DBFC is to demonstrate its reliable, long term operation, which has been rarely addressed in the previous work. In this work, evaluation of the anode durability was carried out by monitoring changes in cell voltage at a current density of 20 mA cm^{-2} during a 50 h operation, as shown in Figure 8. The DBFCs with the mesh anodes can maintain a slightly better performance than those with the carbon anodes, suggesting the better stability of the mesh anodes.

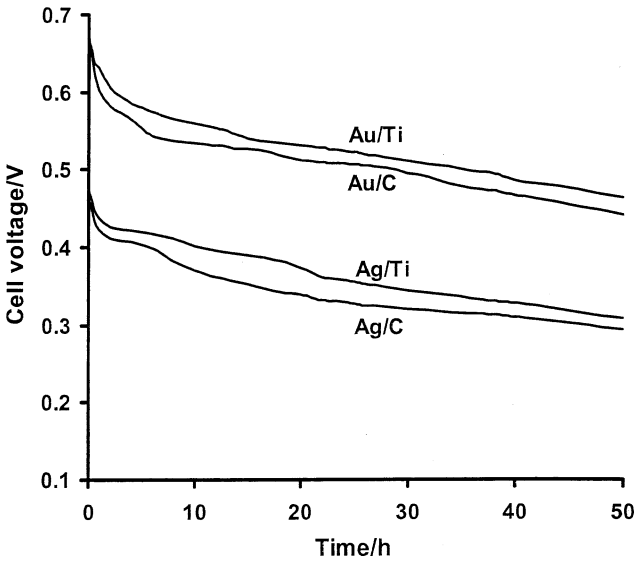

Fig. 8. Durability of the DBFCs with different anodes. Anode catalyst loading: 2 mg metal cm^{-2}. Applied current density: 20 mA cm^{-2}. Temperatures: 25 °C. Other conditions as in Figure 6.

However, the performance decreases with time for all DBFCs. This gradual deterioration may be due to several factors, such as dissolution and agglomeration of the anode catalysts and poisoning catalyst surface. In addition, deactivation of the cathodes and membrane due to formation of NaOH and carbonates at the cathode may also be a factor. The formation of carbonates is associated with the use of Na^+ ion conducting membranes in the presence of air and thus CO_2. The problems may not be a serious issue during a short term operation but becomes severe in a prolonged test unless a mechanism for CO_2 removal and NaOH management is used. The use of alkaline membranes that are OH^- ion conducting may be one solution to the latter problem.

4. Conclusions

The new Ti mesh support for Au and Ag catalysts for $NaBH_4$ oxidation shows superior performance to that obtained with carbon supports. High power densities (up to 92.4 mW cm^{-2}) and modest stability were achieved in the direct borohydride fuel cell with the Au/Ti mesh anode. The optimum DBFC performance can be achieved with an anode loading of 2 mg metal cm^{-2} and a temperature of 85 °C using an aqueous fuel of 1.32 M $NaBH_4$ and 2.5 M NaOH.

The non-precious Ag anode showed reasonably high peak power densities of up to 60 mW cm^{-2}. In terms of economics the use of an Ag anode may prove to be a better material for DBFCs which are used for larger scale power applications. This could be particular benefit if non-precious metal, borohydride tolerant cathodes are used.

Acknowledgements

The authors thank the EPSRC for funding and an EPSRC/HEFCE Joint Infrastructure Fund award (No. JIF4NESCEQ) for research facilities.

References

1. C Ponce de Leon, FC Walsh, D Pletcher, DJ Browning and JB Lakeman, *J Power Sour* **155** (2006) 172.
2. J-H Wee, *J Power Sour* **155** (2006) 329.
3. BH Liu, ZP Li, K Arai and S Suda, *Electrochim Acta* **50** (2005) 3719.
4. A Verma and S Basu, *J Power Sour* **145** (2005) 282.
5. BH Liu, ZP Li and S Suda, *Electrochim Acta* **49** (2004) 3097.
6. ZP Li, BH Liu, K Arai and S Suda, *J Electrochem Soc* **150** (2003) A868.
7. Cheng H, Scott K (available online 29 March 2006) J Power Sour (in press).
8. H Cheng and K Scott, *Electrochim Acta* **51** (2006) 3429.
9. K Wang, J Lu and L Zhuang, *J Electroanal Chem* **585** (2005) 191.
10. H Dong, R Feng, X Ai, Y Cao, H Yang and C Cha, *J Phys Chem B* **109** (2005) 10896.
11. E Gyenge, *Electrochim Acta* **49** (2004) 965.
12. MV Mirkin, H Yang and AJ Bard, *J Electrochem Soc* **139** (1992) 2212.
13. SC Amendola, P Onnerud, MT Kelly, PJ Petillo, SL Sharp-Goldman and M Binder, *J Power Sour* **84** (1999) 130.
14. J-H Kim, H-S Kim, Y-M Kang, M-S Song, S Rajendran, S-C Han, D-H Jung and J-Y Lee, *J Electrochem Soc* **151** (2004) A1039.
15. BH Liu, ZP Li and S Suda, *J Electrochem Soc* **150** (2003) A398.
16. R Jasinski, *Electrochem Tech* **3** (1965) 40.
17. K Kinoshita, *Electrochemical oxygen technology* (John Wiley & Sons, New York, 1992)Chapter 3.
18. CJ Brown, D Pletcher, FC Walsh, JK Hammond and D Robinson, *J Appl Electrochem* **24** (1994) 95.
19. H Cheng and K Scott, *J Power Sour* **123** (2003) 137.
20. C Lim, K Scott, RG Allen and S Roy, *J Appl Electrochem* **24** (2004) 929.
21. RX Feng, H Dong, YD Wang, XP Ai, YL Cao and HX Yang, *Electrochem Commun* **7** (2005) 449.
22. H Cheng, K Scott and PA Christensen, *J Appl Electrochem* **35** (2005) 551.
23. DR Lide and HPR Frederikse (ed.), *CRC handbook of chemistry and physics*, 78rd ed., (CRC Press, New York, 1997)Section 8.
24. N Lingaiah, MA Uddin, A Muto, T Iwamoto, Y Sakata and Y Kusano, *J Mol Catal A: Chem* **161** (2000) 157.
25. http://www.icdd.com/ (the reference code is 04-0784).
26. Hine F (1985) Electrode Processes and Electrochemical Engineering. Plenum Press, New York Chapter 4, p 75.